The Interaction between Pyoverdin and Its Outer Membrane Receptor in *Pseudomonas aeruginosa* Leads to Different Conformers: A Time-Resolved Fluorescence Study†

Nicolas Folschweiller,‡ Jacques Gallay,*,§ Michel Vincent,§ Mohamed A. Abdallah,‡ Franc Pattus,‡ and Isabelle J. Schalk*,‡

ESBS, Ecole Supérieure de Biotechnologie de Strasbourg, UPR CNRS 9050, Bld Sébastien Brant, 67400 Illkirch, France, and LURE, Laboratoire pour l'Utilisation du Rayonnement Electromagnétique, CNRS-CEA-MDRI, Université Paris-Sud, Bâtiment 209D, 91898 Orsay Cedex, France

Received April 16, 2002

ABSTRACT: In iron limitation conditions, *Pseudomonas aeruginosa* secretes a major fluorescent siderophore named pyoverdin (PaA). PaA has an extremely high affinity for Fe^{3+} but also chelates other ions such as Al^{3+} and Ga^{3+} with a lower affinity. The transfer of PaA−Fe^{3+} across the outer membrane of the bacteria is mediated by the receptor FpvA, a TonB-dependent outer membrane transport protein. FpvA binds the iron-free and iron-loaded forms of pyoverdin with similar affinities, but only PaA−Fe^{3+} is taken up by the cell, suggesting that FpvA adopts different conformations depending on its loading status. We used time-resolved fluorescence spectroscopy to characterize the different forms of FpvA−PaA in vitro. We showed that the FpvA−PaA complex adopts two different conformations depending on how it was prepared (formed in vitro or in vivo prior to purification). The dihydroquinoline moiety of both conformers is fully protonated, or coordinated by protein charged groups, but the polarity of its environment, its solvent accessibility, and its rotational dynamics are much slower when the FpvA−PaA complex is formed in vivo than in vitro. In the presence of Ga^{3+} or Al^{3+} ions, the solvent accessibility and mobility of the dihydroquinoline moiety in the two FpvA−PaA complexes are intermediate between those observed for the metal-free ones. In addition, the Förster resonance energy transfer kinetics from FpvA tryptophan residues to the PaA chromophore differs from one complex to the other, revealing differences in one or more of the donor−acceptor topologies.

Fluorescent *Pseudomonas* are bacteria characterized by the overproduction under iron-deficient conditions of yellow-green, water-soluble biopeptides, called pyoverdins, displaying a high affinity for Fe^{3+}. Pyoverdins have a low molecular mass (1000−1500 Da), and all contain the same highly fluorescent chromophore, which is derived from 2,3-diamino-6,7-dihydroxyquinoline, containing one of the bidentate groups involved in iron chelation. This chromophore is linked to a peptidic moiety, containing the other two bidentate groups required for Fe^{3+}. The size and amino acid composition of pyoverdins are unique to each species of *Pseudomonas*, indicating specialization by each bacterium of its pyoverdin.

Pseudomonas aeruginosa ATCC 15692 produces the pyoverdin represented in Figure 1. Its outer membrane receptor, FpvA,[1] a TonB-dependent receptor, has been cloned and sequenced (*1*). In a similar way as with other TonB-dependent uptake systems, the process of iron uptake by the bacterium begins with the binding of a siderophore−ferric complex, PaA−Fe^{3+}, to its specific outer membrane receptor, FpvA. The next step is the translocation of the iron-loaded siderophore to the periplasm. This probably occurs via the FpvA receptor, but the pathway involved has not been elucidated. This process requires energy, which is provided

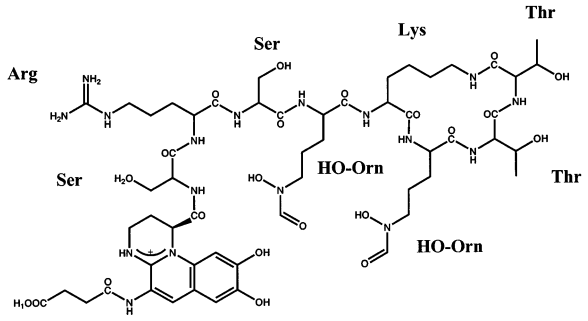

FIGURE 1: Chemical structure of PaA.

† This work was partly funded by the Centre National de la Recherche Scientifique (Programme Physique et Chimie du Vivant, 2000).

* To whom correspondence should be addressed. I.J.S.: e-mail, schalk@esbs.u-strasbg.fr; phone, (+33) (0) 3 90 24 47 31; fax, (+33) (0) 3 90 24 48 29. J.G.: e-mail, jacques.gallay@lure.u-psud.fr; phone/fax, (+33) (0) 1 64 46 80 82.

‡ ESBS, Ecole Supérieure de Biotechnologie de Strasbourg, UPR CNRS 9050.

§ LURE, Laboratoire pour l'Utilisation du Rayonnement Electromagnétique, CNRS-CEA-MDRI, Université Paris-Sud.

[1] Abbreviations: FRET, Förster resonance energy transfer; MEM, maximum entropy method; octyl POE, octyl polyoxyethylene; DAS, decay-associated spectra; FpvA, outer membrane receptor of PaA in *Pseudomonas aeruginosa*; PaA, pyoverdine; TonB, a protein which couples the protonmotive force in the cytoplasmic membrane to iron chelate receptors in the outer membrane.

10.1021/bi0259711 CCC: $22.00 © 2002 American Chemical Society
Published on Web 11/14/2002

by a multimeric complex consisting of the inner membrane proteins TonB, ExbB, and ExbD. This complex has been identified in many Gram-negative bacteria. It participates in a conserved mechanism of energy tranduction from the inner membrane to the high-affinity transporters located in the outer membrane, using the protonmotive force (*2*−*7*). Once in the periplasm, a carrier directs the siderophore to a cytoplasm-directed ABC transporter (ATP binding cassette) located in the inner membrane (reviewed in ref *8*).

The three-dimensional structures of FhuA, FepA, and FecA, three FpvA homologues respectively implicated in iron−ferrichrome, iron−enterobactin, and iron−citrate uptake in *Escherichia coli*, have been solved (*9*−*12*). They all consist of a 22-stranded β-barrel, filled by a domain called a "plug" or a "cork". The FhuA−ferrichrome X-ray structure (*9*, *10*) revealed that the ferrichrome binds above the cork and interacts with amino acid residues of the cork and of the β-barrel domains.

In vitro and in vivo studies have shown that the outer membrane receptor FpvA is able to bind iron-free PaA and ferric−PaA with very similar affinities, although only ferric−PaA is taken up by the cell (*13*, *14*). Moreover, the natural form of the FpvA receptor in the absence of iron seems to be the FpvA−PaA complex (*13*, *14*). During iron uptake, the extracellular ferric−PaA displaces the bound PaA on the FpvA receptor to form the FpvA−PaA−Fe^{3+} complex (*15*). The kinetics of the formation of this exchange is regulated by TonB in vivo. It is not known for sure whether the binding of PaA to FpvA in the absence of iron has functional significance. There is some evidence that PaA positively regulates the expression of the *fpvA* gene (*16*) and that FpvA belongs to a subset of siderophore receptors also involved in signal transduction (reviewed in ref *17*). These data strongly suggest that FpvA adopts different conformations depending on its current loading status. The different conformations, with and without iron, may trigger different bacterial responses, directing the uptake or the signal transduction process, respectively.

We studied the effects of pH, temperature, and metal binding on the fluorescence properties of PaA alone in solution. We then characterized the conformation and dynamics of the different FpvA complexes by time-resolved fluorescence spectroscopy in order to investigate in detail the binding properties of FpvA and the way in which purified FpvA interacts with PaA and with PaA−Ga^{3+} and PaA−Al^{3+}, as fluorescent analogues of the nonfluorescent PaA−Fe^{3+}.

MATERIALS AND METHODS

Chemicals. Carbenicillin disodium salt was a generous gift from Smith-Klyne-Beecham (Welwyn Garden City, Herts, U.K.). $^{55}FeCl_3$ was purchased from NEN (Boston, MA). Pyoverdins (PaA, PaA−Fe^{3+}, PaA−Al^{3+}, and PaA−Ga^{3+}) were prepared as described previously (*18*, *19*). Tritiated PaA−Fe^{3+}, PaA−Al^{3+}, and PaA−Ga^{3+} were made by mixing 1 equiv of $FeCl_3$, 3 equiv of $AlCl_3$ or 3 equiv of $Ga(NO_3)_3$, respectively, with 1 equiv of [^{3}H]PaA in water. The mixture was incubated for 15 min and used without further purification.

Bacterial Strains and Growth Media. The strains used in this study were the wild-type strain *P. aeruginosa* ATCC 15692 and two mutants: CDC5(pPVR2), an FpvA-overproducing and PaA-deficient strain (*20*), and K691(pPVR2), an FpvA-overproducing and PaA-producing strain (*1*). All strains were grown overnight at 29 °C to an OD_{600} of 1.0 in succinate medium (*18*) supplemented with 150 μg/mL carbenicillin for strains CDC5(pPVR2) and K691(pPVR2).

Distribution of Radiolabeled PaA in P. aeruginosa. P. aeruginosa ATCC 15692 cells were incubated with [^{3}H]PaA, [^{3}H]PaA−Fe^{3+}, [^{3}H]PaA−Ga^{3+}, or [^{3}H]PaA−Al^{3+} for 5 min, and the distribution of [^{3}H]PaA between the extracellular medium, membrane fractions (inner and outer membranes), and soluble fraction (periplasm and cytoplasm) was determined as described previously (*15*).

Purification of FpvA and FpvA−PaA and in Vitro Preparation of FpvA−PaA and FpvA−PaA−Metal Ion Complexes. FpvA was purified from CDC5(pPVR2), and the FpvA−PaA complex (copurified complex) was purified from K691(pPVR2) as described by Schalk et al. (*13*). Both strains carry a copy of the *fpvA* gene on the multicopy plasmid pPVR2. To prepare in vitro the different FpvA−siderophore complexes, 0.6 μM purified FpvA was incubated for 1 h at room temperature in the presence of 0.6 μM PaA, PaA−Ga^{3+}, or PaA−Al^{3+} in 50 mM Tris-HCl, pH 8.5, and 1% octyl POE.

Ligand Binding Assays. For the in vitro determination of the inhibition constant of PaA−Ga^{3+} and PaA−Al^{3+} to purified FpvA, we used the filtration assay developed previously for purified FpvA (*13*).

Steady-State and Time-Resolved Fluorescence Measurements. Corrected steady-state fluorescence excitation and emission spectra and steady-state anisotropies were recorded on an SLM 8000 spectrofluorometer. Cryogenic experimental conditions were obtained with a variable temperature Janis cryostat, VPF-100 (Janis Research Co., Wilmington, MA).

Fluorescence intensity and anisotropy decays were obtained from the polarized components $I_{vv}(t)$ and $I_{vh}(t)$ by the time-correlated single-photon-counting technique. For tryptophan−PaA energy transfer measurements at 295 nm for excitation wavelength conditions, the experimental setup installed on the SB_1 window of the synchrotron radiation Super-ACO machine (Anneau de Collision d'Orsay), working at a repetition rate of 8.33 MHz, was used. The pulse width at half-maximum was 600−700 ps. The excitation wavelength was selected by a double monochromator (Jobin Yvon UV-DH10, bandwidth 4 nm). For direct excitation of PaA at 400 nm, the light pulse of a blue diode laser LDH400 from Picoquant (Berlin-Adlershof, Germany) was used. The diode laser was used at a repetition rate of 10 MHz. The instrument response function (~300 ps) was monitored with the picosecond scintillator lifetime standard 4-(dimethylamino)-4′-cyanostilbene (DCS) (τ = 41 ps in cyclohexane). In both cases fluorescence emission was selected by a single monochromator (Jobin Yvon UV-H10, bandwidth 8 nm). A MCP-PMT Hamamatsu detector (model R3809U-02) was used. The time resolution was ~20 ps per channel, and the data were stored in 2048 channels. Automatic sampling cycles including 30 s accumulation time for the instrument response function and 90 s for each polarized component were carried out until a total number of 2−10 million counts was reached in the fluorescence intensity decay.

Table 1: Fluorescence Emission Parameters (Maximum Emission Wavelength λ_{max}, Excited-State Lifetime τ_i, and Their Amplitudes α_i) of PaA in Different Conditions[a]

sample	λ_{max} (nm)	τ_1 (ns)	τ_2 (ns)	τ_3 (ns)	α_1	α_2	α_3	$\langle\tau\rangle$ (ns)
PaA, pH 9		5.92	3.32	0.84	0.08	0.62	0.30	2.79
PaA, pH 8.5	450	3.95	1.83	0.75	0.49	0.23	0.28	2.56
PaA, pH 7	450	5.25 ± 0.61	2.08 ± 0.17	0.74 ± 0.13	0.41 ± 0.11	0.24 ± 0.09	0.36 ± 0.04	2.94 ± 0.60
PaA, p^2H 7		4.91 ± 0.10	2.52 ± 0.50	0.99 ± 0.10	0.68 ± 0.06	0.16 ± 0.02	0.16 ± 0.02	3.92 ± 0.01
PaA, pH 5		6.10 ± 0.02	2.17 ± 0.16	0.60 ± 0.04	0.62 ± 0.01	0.20 ± 0.01	0.18 ± 0.02	4.37 ± 0.01
PaA, pH 4	452	6.46		0.6	0.96		0.04	6.22
PaA$-Ga^{3+}$	457	6.33		1.3	0.95		0.05	6.09
PaA$-Al^{3+}$	457	6.45		0.8	0.95		0.05	6.20
PaA$-Ga^{3+}$; glycerol, 75% w/w; 20 °C	458	6.0	2.1	0.4	0.78	0.06	0.16	4.88
PaA$-Ga^{3+}$; glycerol, 75% w/w; −50 °C	450	nd	nd	nd	nd	nd	nd	nd
in vivo formed FpvA−PaA complex	445	6.85 ± 0.10	1.81 ± 0.52	0.84 ± 0.11	0.93 ± 0.03	0.03 ± 0.01	0.04 ± 0.02	6.46 ± 0.02
in vitro formed FpvA−PaA complex	451	6.89 ± 0.03	1.67 ± 0.36		0.95 ± 0.01	0.05 ± 0.01		6.62 ± 0.02
in vitro formed FpvA−PaA$-Ga^{3+}$ complex	445	6.68 ± 0.03	1.83 ± 0.35		0.96 ± 0.01	0.04 ± 0.01		6.42 ± 0.04
in vitro formed FpvA−PaA$-Al^{3+}$ complex	447	7.18 ± 0.06	1.96 ± 0.14		0.93 ± 0.01	0.07 ± 0.01		6.82 ± 0.06

[a] MEM analysis was performed on the fluorescence intensity $S(t)$ independent of polarization reconstructed from the parallel and perpendicular polarized components $I_{vv}(t)$ and $I_{vh}(t)$ such as $S(t) = I_{vv}(t) + 2GI_{vh}(t) = \int_0^\infty \alpha(t) \exp(-t/\tau)\, d\tau$, where τ is the excited-state lifetime, $\alpha(\tau)$ is its normalized amplitude distribution, and G is a correction factor accounting for the difference in transmission of the $I_{vv}(t)$ and $I_{vh}(t)$ components. τ_i and α_i are respectively the values of the center and of the integrated normalized amplitudes of each lifetime peak. The mean lifetime $\langle\tau\rangle$ is calculated as $\langle\tau\rangle = \sum_i \alpha_i \tau_i$. Standard deviations for three to four measurements are shown.

The fluorescence intensity decays were analyzed as sums of exponentials by the maximum entropy method (*21*, *22*). MEMSYS 5 (MEDC Ltd., U.K.) was used as a library of subroutines. Sets of 150 lifetime values, equally spaced on a log scale, were used. In the case of FRET, the evolution and decay of acceptor fluorescence excited via donors were analyzed using a model including no a priori condition on the preexponential sign (*23*). Fluorescence anisotropy decays were analyzed as the sum of exponential terms (*22*) using sets of 100 correlation time values, equally spaced on a log scale.

RESULTS

PaA$-Ga^{3+}$ and PaA$-Al^{3+}$ Bind to FpvA and Are Taken Up by P. aeruginosa. Upon binding to PaA, ferric iron completely quenches the fluorescence of the PaA chromophore, so the PaA$-Fe^{3+}$ complex cannot be used as a fluorescent probe. However, PaA$-Al^{3+}$ and PaA$-Ga^{3+}$ complexes are strongly fluorescent and may appropriately be used as PaA$-Fe^{3+}$ analogues for FRET, provided that their binding and uptake properties are similar. To determine whether the fluorescent PaA$-Al^{3+}$ and PaA$-Ga^{3+}$ complexes are transported like PaA$-Fe^{3+}$ by the bacterium, we incubated *P. aeruginosa* ATCC 15692 cells with 50 nM [^{3}H]-PaA, [^{3}H]PaA$-Fe^{3+}$, [^{3}H]PaA$-Ga^{3+}$, or [^{3}H]PaA$-Al^{3+}$ for 5 min and measured the cellular distribution of radioactivity.

As shown previously (*18*), [^{3}H]PaA was not taken up. Nearly all (99%) of the radioactivity was lost during cell washing, and less than 0.1% was internalized. With [^{3}H]-PaA$-Fe^{3+}$, 9% of the radioactivity was found either bound to the inner membrane or in the soluble fraction (periplasm + cytoplasm). With [^{3}H]PaA$-Ga^{3+}$ and [^{3}H]PaA$-Al^{3+}$, 13% and 3% of the radioactivity, respectively, was internalized after 5 min, clearly demonstrating that PaA$-Ga^{3+}$ and PaA$-Al^{3+}$ are taken up by *P. aeruginosa*. Moreover, the uptake rates were comparable for PaA$-Ga^{3+}$ and PaA$-Fe^{3+}$ but slower for PaA$-Al^{3+}$. This is consistent with PaA$-Fe^{3+}$ and PaA$-Ga^{3+}$ having a similar inhibition constant for purified FpvA, 7.5 nM (*13*) and 16 nM (this work), respectively, whereas PaA$-Al^{3+}$ has a much higher inhibition constant (350 nM). Ion size may also explain why Al^{3+} is less efficiently transported than the other ions.

Effect of pH, Metal Binding, and Temperature on the Fluorescence Properties of PaA in Solution. Spectroscopic titration of the aposiderophore revealed three pH-dependent absorbing species, corresponding to the three protonation states of the dihydroquinoline-type chromophore (*19*) ($pK_1 = 5.7$; $pK_2 = 10.8$). The fluorescence emission properties of the chromophore were also sensitive to pH and to the presence of the metal. The fluorescence emission spectrum exhibited a maximum near 450 nm at pH 8.5. It was red shifted by ~2 nm at pH 4 and by 7 nm upon metal ion binding at pH 8.5 (Al^{3+} or Ga^{3+}) (Table 1). The fluorescence decay was strongly affected in this pH range. At pH 4, corresponding to the fully protonated form (*19*), it was almost monoexponential (Figure 2A,B) with a long lifetime (~6 ns) corresponding to 96% of the initially excited population (Table 1). At higher pH values, the fluorescence decay becomes multiexponential (Figure 2C and Table 1). Three lifetime populations are detected, whose respective amplitudes and center values depend on pH. The variation of the mean lifetime (defined in the legend of Table 1) as a function of pH follows a sigmoid curve (Figure 3). It exhibits a first curvature around pH 5.5, corresponding roughly to pK_1 (*19*), and a second one at pH above 9 due to pK_2. At pH >10, the chromophore becomes unstable, precluding any measurement. These data clearly show that the fluorescence emission state of the dihydroquinoline depends on the ionization state of the catechol group.

To assess whether a proton transfer with the solvent could be responsible for this pH effect on the lifetime distribution, measurements in D_2O were performed. No obvious solvent isotope effect could however be observed on the lifetime values (Table 1), which should occur in the case of a nonradiative deactivation mechanism involving a proton transfer with the solvent (*24*). The relative amplitudes of the lifetime population are nevertheless affected; the amplitude of the long lifetime increases significantly with respect to that at neutral pH in H_2O (Table 1). The acidic pK_1 of the catechol group is probably increased in D_2O, thereby increasing the concentration of the uncharged form in this solvent with respect to H_2O at neutral pH.

Further insight in the fluorescence heterogeneity of the charged species of the dihydroquinoline moiety can be

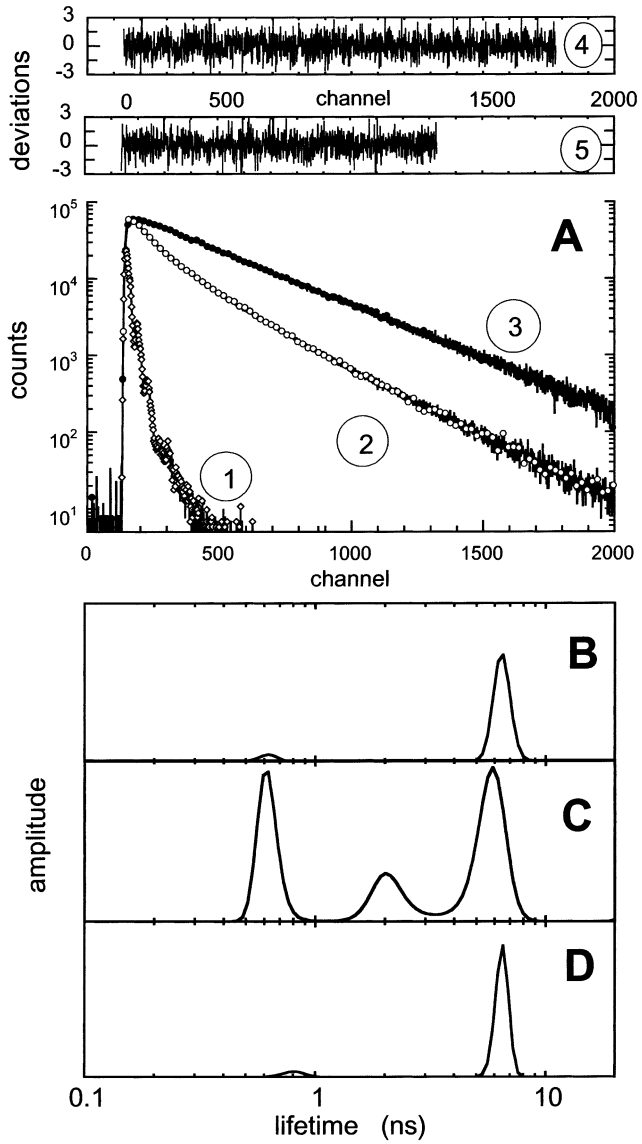

FIGURE 2: Fluorescence intensity decay of PaA. (A) Experimental decay: (1) instrumental response function; (2) fluorescence intensity decay of PaA at pH 7; (3) fluorescence intensity decay of PaA at pH 4; (4) plot of the weighted residuals corresponding to decay curve 2; (5) plot of the weighted residuals corresponding to decay curve 3. (B) MEM recovered excited-state lifetime distribution of PaA at pH 4. (C) MEM recovered excited-state lifetime distribution of PaA at pH 7. (D) MEM recovered excited-state lifetime distribution of PaA−Al^{3+} at pH 7. Conditions: excitation wavelength, 400 nm; emission wavelength, 450 nm; PaA concentration, 0.5 μM; time resolution, 22 ps/channel.

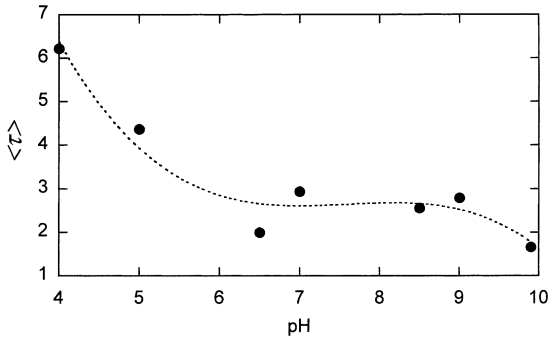

FIGURE 3: Variation of the PaA mean excited-state lifetime as a function of pH: excitation wavelength, 400 nm; emission wavelength, 450 nm.

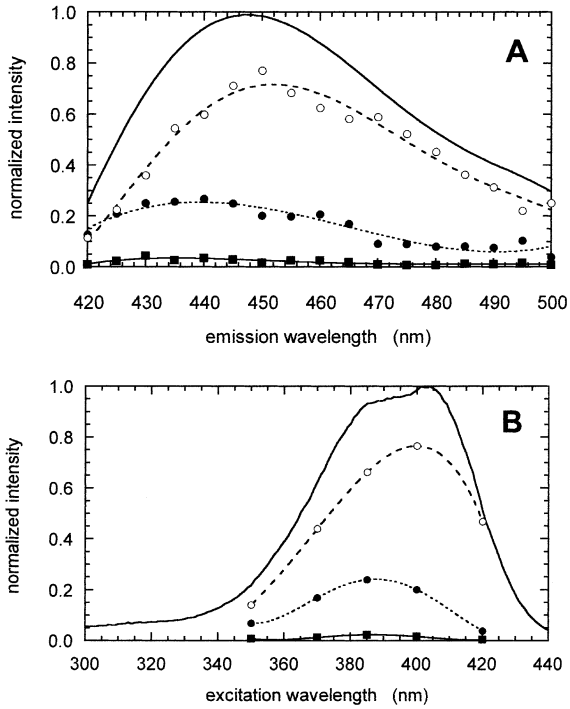

FIGURE 4: Decay-associated spectra of PaA: (A) emission spectra (excitation wavelength, 400 nm); (B) excitation spectra (emission wavelength, 450 nm). Experiments were performed at pH 6.5. Key: (○) long lifetime; (●) intermediate lifetime; (■) short lifetime.

obtained by DAS measurements. These studies at neutral pH show that the two longest lifetimes (responsible for 90% of the fluorescence intensity) display different spectral distributions: the longest lifetime shows a red-shifted DAS (452 nm) with respect to that of the other lifetime (438 nm) (Figure 4A). No excited-state reaction could be detected at long emission wavelength. These two lifetime populations display also different spectral distributions as a function of the excitation wavelength: the longest lifetime is dominant in the 405 nm absorption band, while the second one is dominant in the 385 nm band (Figure 4B). The data suggest therefore that the fluorescence heterogeneity stems from a ground-state heterogeneity associated with different ionization states of the catechol group. At pH 4, only the fully protonated form is present, characterized by a major long lifetime, whereas at neutral pH, where only one of the catechol group is protonated, two ionized forms can coexist by means of an intramolecular proton transfer between these two functions.

The fluorescence decays of the dihydroquinoline chromophore in the PaA−Al^{3+} and PaA−Ga^{3+} complexes either at pH 7 or at pH 8.5 were almost monoexponential with long lifetime values close to those measured at pH 4 in both cases (Figure 2D and Table 1).

The Bound States of PaA and PaA−Metal Ion Complexes to Its FpvA Receptor: Polarity of the Environment, Accessibility to Water-Soluble Solutes, Ionization, and Rotational Dynamics. PaA can bind FpvA either as an apo complex or as a metallic complex. We have previously described various ways of preparing FpvA−PaA complexes (*13*). A stable complex can be purified from a PaA- and FpvA-producing strain. In this case the FpvA−PaA complex is preformed in vivo and remains in this form during all of the purification

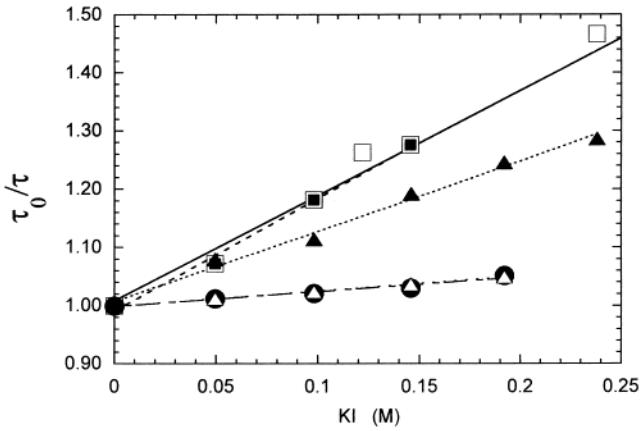

FIGURE 5: Stern−Volmer plot of (τ_0/τ) as a function of iodide concentration: (■) PaA at pH 4; (□) PaA−Ga^{3+} complex at pH 7; (△) FpvA−PaA in vivo formed complex; (●) FpvA−PaA−Ga^{3+} complex; (▲) FpvA−PaA in vitro formed complex. A stock solution of 5 M KI containing 0.1 mM $Na_2S_2O_3$ was used. Conditions: excitation wavelength, 400 nm; emission wavelength, 445 nm. The measurements for all FpvA−PaA complexes were performed at pH 8.5.

steps. Alternatively, FpvA can be purified from a PaA-deficient strain and subsequently incubated with PaA or PaA−metal ion complexes to form binary FpvA−PaA and ternary FpvA−PaA−metal complexes, respectively. We measured the fluorescence properties of the chromophore to characterize these different FpvA complexes.

The copurified FpvA−PaA complex fluorescence exhibits a significantly blue-shifted emission spectrum regarding apo-PaA in buffer (Table 1). This blue shift is likely due to solvatochromic properties of the dihydroquinoline moiety, as suggested by the temperature effect on the fluorescence spectrum of the PaA−Ga^{3+} complex: at −50 °C in 75% w/w glycerol/water, it was blue shifted by 8 nm with respect to that at room temperature (Table 1). This effect is similar but smaller in amplitude to that observed with other polarity-sensitive probes (*23*, *25*, *26*). It is likely due to the immobilization of the solvent dipoles close to the chromophore, which cannot relax anymore around the excited state. This suggests that the siderophore is located in a hydrophobic cavity within the receptor. FpvA−PaA−Al^{3+} and FpvA−PaA−Ga^{3+} complexes that had been formed in vitro both exhibited the same fluorescence emission spectrum as the in vivo formed FpvA−PaA complex. However, the emission maximum was significantly blue shifted with respect to that of PaA−Al^{3+} and PaA−Ga^{3+} in buffer (Table 1). In contrast, the FpvA−PaA complex formed in vitro did not exhibit this shift, suggesting a more polar environment compared to the three other complexes (copurified FpvA−PaA, FpvA−PaA−Ga^{3+}, and FpvA−PaA−Al^{3+}).

The fluorescence decay of the chromophore in all of the FpvA−PaA complexes is governed by a major lifetime component, whose value is similar to that recorded at pH 4 and in the metal-loaded PaA (Table 1). This suggests that the catechol is either fully protonated or bound to counter charges in the receptor binding site.

The degree of accessibility of the fluorescent ring to water-soluble solutes for the different complexes was estimated by fluorescence quenching experiments with iodide (*27*). Linear Stern−Volmer plots were obtained (Figure 5), and Stern−Volmer constants K_{sv} were determined (Table 2). The

Table 2: Stern−Volmer Iodide Quenching Parameters[a]

sample	K_{sv} (M^{-1})	k_q (M^{-1} s^{-1})
PaA, pH 4	1.93	3×10^8
PaA−Ga^{3+}	1.80	2.8×10^8
copurified FpvA−PaA complex	0.26	3.8×10^7
in vitro formed FpvA−PaA complex	1.21	1.8×10^8
in vitro FpvA−PaA−Ga^{3+} complex	0.25	3.7×10^7

[a] K_{sv} is the Stern−Volmer constant given by the slope of the linear plot τ_0/τ versus [I^-] (τ_0 and τ are the longest excited-state lifetime values in the absence and in the presence of I^-, respectively). k_q is the bimolecular quenching constant: $k_q = K_{sv}/\tau_1$. Conditions: excitation wavelength, 400 nm; emission wavelength, 450 nm.

bimolecular quenching constant k_q of iodide was compared to that for PaA in pH 4 buffer and for PaA−Ga^{3+}. The results show that k_q is 6−7 times lower for the copurified FpvA−PaA complex than for PaA or PaA−Ga^{3+} solution (Table 2) [accessibility of less than 10% according to Johnson and Yguerabide (*28*)]. A similar k_q value is obtained for the FpvA−PaA−Gal^{3+} complex, but it is significantly higher for the in vitro formed FpvA−PaA complex (Table 2). This suggests that the accessibility to the water-soluble solute of the dihydroquinoline moiety in the in vitro formed FpvA−PaA is significantly higher than in FpvA−PaA−Ga^{3+} or in the copurified FpvA−PaA complexes.

The mobility of PaA bound to FpvA in the different complexes was studied by time-resolved fluorescence anisotropy. The internal mobility is weak in the in vivo formed complex as shown by the experimental anisotropy decay, which essentially displays a major, slow time component (Figure 6A, curve 2), which is much slower than that of free PaA (Figure 6A,B). Two rotational correlation times were measured (Figure 6C). The longest one dominated the decay and described the Brownian rotation of the complex (Table 3). The shortest one, much longer than the Brownian rotational correlation time of the free PaA (Figure 6B), describes likely the motion of the chromophore within the receptor binding cavity. Faster irresolvable motions exist, however, as the initial anisotropy value ($r_{t=0}$) is smaller than that measured in vitrified medium ($r_0 = 0.394 \pm 0.002$) under the same excitation and emission wavelength conditions. Their combined amplitudes are low, as reflected in the correspondingly small values of wobbling-in-cone angles ω_{max} (Table 3). The amplitude of the chromophore internal mobility was larger for the in vitro prepared complexes, whether the metal is present or not (Table 3).

Topology of the Siderophore Bound to FpvA: Trp−PaA Förster Resonance Energy Transfer (FRET) in the FpvA−PaA, FpvA−PaA−Al^{3+}, and FpvA−PaA−Ga^{3+} Complexes. FRET between donor tryptophan residues and the dihydroquinoline moiety (*13*) can be used as a "spectroscopic ruler" (*29*) to further characterize the topology of the PaA molecule in the different complexes. FRET occurs because the red edge of the Trp emission and the blue edge of the PaA absorption spectra display an overlap (Figure 7A). The calculated value of the overlap integral J_λ is 7.1×10^{-15} M^{-1} cm^3, using a value of 19000 M^{-1} cm^{-1} as the extinction coefficient of PaA at 400 nm (*13*).

To estimate the transfer efficiency, which can provide in principle geometrical information on the complexes, we monitored the steady-state fluorescence excitation spectra of PaA in the different complexes to detect possible changes

Table 3: Fluorescence Anisotropy Decay Parameters of PaA in Solution and in the Different Complexes with the FpvA Receptor[a]

sample	θ_1 (ns)	θ_2 (ns)	β_1	β_2	ω_{max} (deg)	r_{ss}
PaA, pH 4		0.67 ± 0.08		0.323 ± 0.028	21 ± 4	
PaA−Al^{3+}		0.80 ± 0.09		0.355 ± 0.012	15 ± 2	
PaA−Ga^{3+}		0.97 ± 0.03		0.345 ± 0.008	17 ± 1	
copurified FpvA−PaA	3.4 ± 1.9	116 ± 15	0.003 ± 0.003	0.373 ± 0.009	11 ± 2	0.357 ± 0.010
in vitro formed FpvA−PaA complex		119 ± 8		0.348 ± 0.012	16 ± 3	0.338 ± 0.014
in vitro formed FvpA−PaA−Ga^{3+} complex	2.1 ± 0.6	132 ± 19	0.028 ± 0.011	0.334 ± 0.009	19 ± 3	0.334 ± 0.014
in vitro formed FvpA−PaA−Al^{3+} complex	7 ± 4	113 ± 37	0.024 ± 0.014	0.350 ± 0.009	16 ± 3	0.344 ± 0.006

[a] The fluorescence anisotropy is assumed to be described by a sum of exponentials: $r(t) = [I_{vv}(t) - GI_{vh}(t)]/[I_{vv}(t) + 2GI_{vh}(t)] = \sum_i \beta_i \exp(-t/\theta_i)$. G is a correction factor accounting for the difference in transmission of the $I_{vv}(t)$ and $I_{vh}(t)$ components. The θ and β coefficients are respectively the values of the center and partial anisotropy of each rotational correlation time peak. The wobbling-in-cone angle ω_{max} was calculated from $\beta_2/r_0 = [^1/_2 \cos \omega_{max}(1 + \cos \omega_{max})]^2$ (*41*) using a value of the intrinsic anisotropy r_0 of 0.394, measured in vitrified medium (glycerol, 75% w/w, at −50 °C). r_{ss} is the steady-state fluorescence anisotropy.

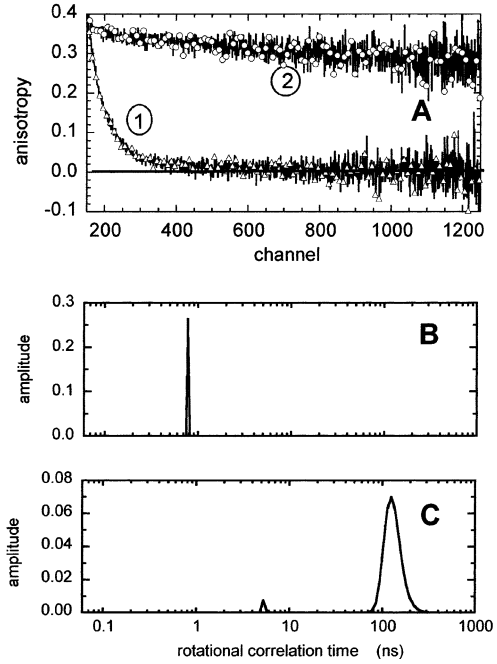

FIGURE 6: Fluorescence anisotropy decays of PaA. (A) Experimental decays: (1) PaA in buffer, pH 4; (2) in vivo formed FpvA−PaA complex. (B) Rotational correlation time distribution for PaA in buffer, pH 4. (C) Rotational correlation time distribution for the in vivo formed FpvA−PaA complex. Conditions: excitation wavelength, 400 nm; emission wavelength, 445 nm; time resolution, 22 ps/channel.

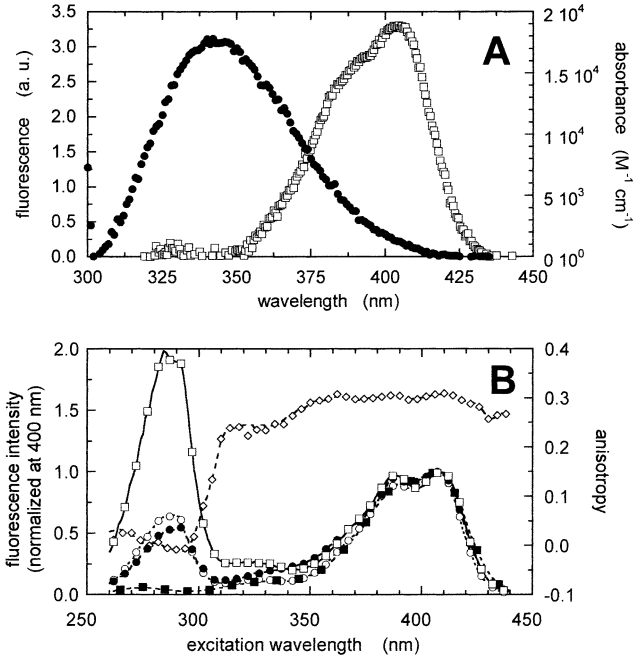

FIGURE 7: (A) Spectral overlap of the Trp emission and PaA absorption spectra: (●) Trp emission spectrum (excitation wavelength, 295 nm); (□) PaA excitation spectrum (emission wavelength, 450 nm). (B) Fluorescence excitation spectra of PaA in different conditions: (■) PaA−Ga^{3+}; (□) in vivo formed FpvA−PaA complex; (●) in vitro formed FpvA−PaA complex; (○) FpvA−PaA−Ga^{3+} complex. All spectra were normalized at 408 nm. (◇) Steady-state anisotropy spectrum of the in vivo formed FpvA−PaA complex. Conditions: protein and PaA concentrations, 0.52 μM at pH 8.5; emission wavelength, 450 nm.

in the amplitude of the Trp excitation band, which could reveal changes in the FRET efficiency. This kind of measurement is particularly convenient in this case since (i) only weak excitation of the acceptor occurs in the absorption band of the donor tryptophan (Figure 7B) and (ii) no residual fluorescence of the donor is measurable at the maximum of emission of the acceptor (440−450 nm) (Figure 7A). As a second kind of experiment, we monitored the tryptophan donor decays in the absence and presence of the acceptor PaA (loaded or not with the metal ion), but the large number of Trp residues in FpvA (17) precludes direct measurements of the FRET kinetics. At the opposite, specific measurements of this kinetics can however be performed by a third type of experiment using time-resolved measurements of acceptor fluorescence sensitized by excitation of the donor(s).

The fluorescence excitation spectrum of the dihydroquinoline chromophore of the in vivo FpvA−PaA copurified complex displayed an intense band at 280−290 nm, which is very weak in the excitation spectrum of the apo-PaA alone or of its complex with the metal in buffer, pH 8.5 (Figure 7B). This band characterizes the efficient transfer of excitation energy from tryptophans to the dihydroquinoline chromophore. The intensity ratio of the excitation band at 290 nm versus that at 400 nm was about 2, compared to 0.05 for PaA in buffer. This ratio was lower for the FpvA−PaA, FpvA−PaA−Al^{3+}, and FpvA−PaA−Ga^{3+} complexes formed in vitro at a molar ratio of ∼1/1, suggesting lower energy transfer efficiencies in these two last cases. This change cannot be due to the residual emission of the donor at the acceptor emission as shown by the emission spectrum of the Trp residues (Figure 7A) but suggests it can likely be ascribed to differences in FRET efficiencies, involving one or more Trp donors.

The second set of experiments consisted in measuring the decay of the tryptophan emission. As expected, the decay

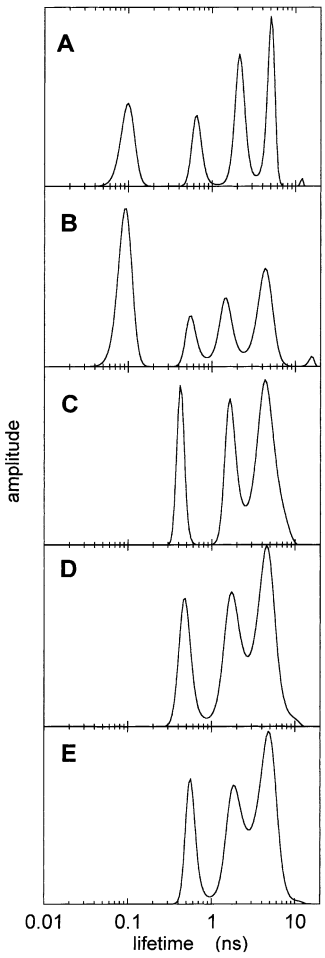

FIGURE 8: MEM recovered excited-state lifetime distribution of the Trp emission. (A) Uncomplexed FpvA: $\tau_1 = 4.74 \pm 0.11$ ns; $\tau_2 = 1.94 \pm 0.33$ ns; $\tau_3 = 0.52 \pm 0.22$ ns; $\tau_4 = 0.11 \pm 0.02$ ns; $\alpha_1 = 0.27 \pm 0.04$; $\alpha_2 = 0.26 \pm 0.06$; $\alpha_3 = 0.17 \pm 0.01$; $\alpha_4 = 0.32 \pm 0.09$. (B) In vitro formed FpvA−PaA complex: $\tau_1 = 4.31$ ns; $\tau_2 = 1.49$ ns; $\tau_3 = 0.58$ ns; $\tau_4 = 0.09$ ns; $\alpha_1 = 0.29$; $\alpha_2 = 0.19$; $\alpha_3 = 0.11$; $\alpha_4 = 0.41$. (C) In vivo formed FpvA−PaA complex: $\tau_1 = 4.24 \pm 0.02$ ns; $\tau_2 = 1.54 \pm 0.25$ 3 ns; $\tau_3 = 0.37 \pm 0.08$ ns; $\alpha_1 = 0.43 \pm 0.04$; $\alpha_2 = 0.33 \pm 0.04$; $\alpha_3 = 0.24 \pm 0.04$. (D) FpvA−PaA−Ga^{3+} complex: $\tau_1 = 4.73$ ns; $\tau_2 = 1.82$ ns; $\tau_3 = 0.50$ ns; $\alpha_1 = 0.46$; $\alpha_2 = 0.32$; $\alpha_3 = 0.22$. (E) FpvA−PaA−Al^{3+} complex: $\tau_1 = 4.76$ ns; $\tau_2 = 1.91$ ns; $\tau_3 = 0.58$ ns; $\alpha_1 = 0.50$; $\alpha_2 = 0.31$; $\alpha_3 = 0.19$. Conditions: excitation wavelength, 295 nm; emission wavelength, 335 nm.

of these 17 Trps in FpvA devoid of PaA is complex but can be fit by four lifetime populations (Figure 8A). In the in vitro formed FpvA−PaA complex, four lifetime populations are again observed; the longest lifetime values are close to those for uncomplexed FpvA, while the shortest one decreases to a value at the limit of the instrument and is more weighted in the complex (Figure 8B). The mean excited-state lifetime decreases to 1.63 ns. In the in vivo formed FpvA−PaA complex, as well as in the FpvA−PaA−metal complexes, the decays are fit by only three lifetime populations: the shortest lifetime population is not detected anymore by the instrument (Figure 8C−E). Moreover, the three remaining populations display shorter lifetime values than in the receptor alone. Overall, the mean lifetime increases from 1.96 for FpvA to 2.42, 2.87, and to 3.07 ns in the copurified FpvA−PaA, in the FpvA−PaA−Ga^{3+}, and in the FpvA−PaA−Al^{3+} complexes, respectively, while the

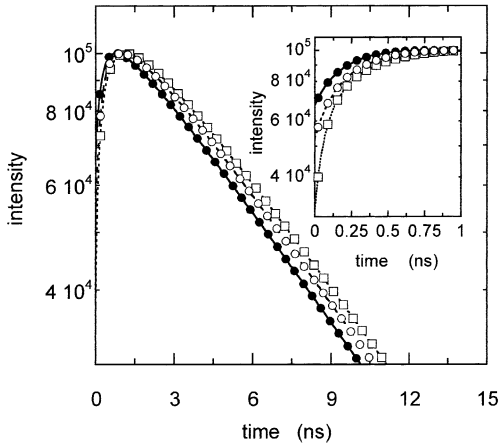

FIGURE 9: Impulse fluorescence decays of PaA after excitation of the donor Trps: (□) in vivo formed FpvA−PaA complex; (●) in vitro formed FpvA−PaA complex; (○) FpvA−PaA−Ga^{3+} complex. Conditions: excitation wavelength, 295 nm; emission wavelength, 440 nm; protein concentration, 0.52 μM. Inset: Rising part of the impulse fluorescence decays expanded on a shorter time scale.

steady-state intensity decreases by ~17% as shown previously (*14*). This behavior suggests that the major FRET process should be very fast, leading to a kind of static quenching. Whether these effects are only due to the FRET process or to the indirect influence of PaA binding on the environment of some Trp residues or both remains an open question. The direct measurement of the energy transfer kinetics can bring some elements to the interpretation of these data. They can provide an estimation of the order of magnitude of the time scale of the transfer process regarding that of the fluorescence emission kinetics and may therefore allow an estimation of the effect of this process on the Trp lifetime distribution.

The time course of the energy transfer was measured directly by monitoring the decay of the dihydroquinoline acceptor at 450 nm after excitation of the donor Trp(s) at 295 nm. As mentioned already, the excitation spectrum of the dihydroquinoline chromophore exhibits a trough in the absorption spectral region of the Trp residues (Figure 7B), implying that the acceptor is essentially only indirectly excited at 290−300 nm. Moreover, no residual fluorescence signal of the donor can be observed at the emission maximum of the acceptor where the measurements were monitored (Figure 7A), so that the acceptor decay kinetics is only due to FRET in these conditions. It displays the unique properties of an excited-state reaction, such as dipolar relaxation or excimer formation (*30*), characterized by a rise in the initial part of the acceptor intensity decay, which can be described by negative preexponential term(s). Accordingly, the impulse fluorescence curves of PaA in the FpvA−PaA complexes excited at 295 nm show a rapidly rising initial evolution (Figure 9), followed by the emission decay of the PaA chromophore. The fastest build-up kinetics was observed for the copurified FpvA−PaA, followed by FpvA−PaA−Ga and by the in vitro formed FpvA−PaA (Figure 9).

A fit of the acceptor experimental decay curves by MEM using a model allowing only positive preexponential terms does not satisfactorily describe the experimental data. The goodness of fit criteria (comparison of χ^2 values and visual inspection of the deviation function) clearly indicate the

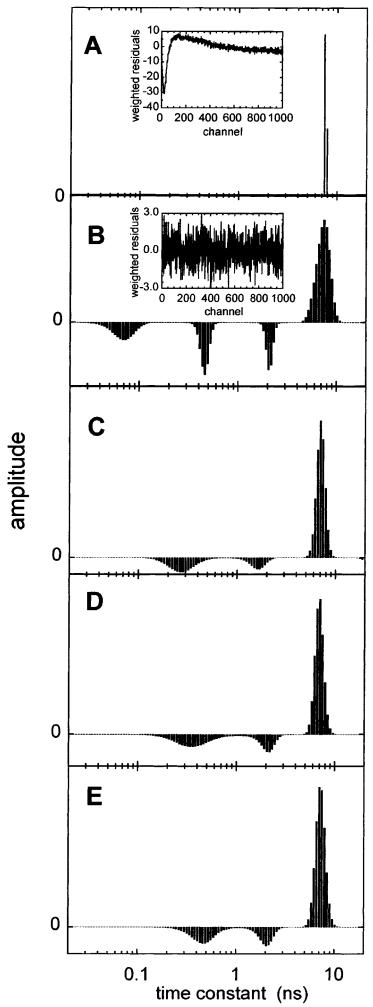

FIGURE 10: MEM recovered time constant distributions of the PaA fluorescence emission excited in the absorption band of the tryptophan residues of FpvA: (A) in vivo formed FpvA−PaA complex analyzed with a model allowing only positive amplitudes (insert: corresponding deviation function); (B) in vivo formed FpvA−PaA complex analyzed with a model allowing both positive and negative amplitudes (insert: corresponding deviation function); (C) in vitro formed FpvA−PaA complex; (D) FpvA−PaA−Ga^{3+} complex; (E) FpvA−PaA−Al^{3+} complex. Conditions: excitation wavelength, 295 nm; emission wavelength, 440 nm. The values of the centers of gravity of the peaks with negative amplitudes represent the harmonic sums of the time constants describing the energy transfer process and of the excited-state lifetime of the donor without acceptor (*42*). These values are the following: for the in vivo formed FpvA−PaA complex, 0.11 ± 0.05 ns, 0.51 ± 0.05 ns, 1.94 ± 0.12 ns; for the in vitro formed FpvA−PaA complex, 0.29 ± 0.01 ns, 1.61 ± 0.01 ns; for the FpvA−PaA−Ga^{3+} complex, 0.34 ± 0.06 ns, 1.82 ± 0.29 ns; and for the FpvA−PaA−Al^{3+} complex, 0.39 ± 0.12 ns, 1.84 ± 0.23 ns. The lifetime peaks of positive amplitudes correspond to the emission of the acceptor (*42*). The values of their center of gravity are respectively 6.94 ± 0.01 ns for curve A, 6.89 ± 0.04 ns for curve B, 6.68 ± 0.03 ns for curve C, and 7.18 ± 0.05 ns for curve D. We can remark that no lifetime peak corresponding to Trp emission can be detected.

requirement for negative terms (Figure 10A,B). A multiexponential fluorescence build-up kinetics, which can be assigned to multiple energy transfer processes owing to the existence of a number of different potential donors, is observed. The time constants correspond to the harmonic sums of the transfer time constants and of the excited lifetime of the donor in the absence of the acceptor. Three time constants are detected for the copurified FpvA−PaA complex (Figure 10B) and only two for the other complexes (Figure 10C−E). More than 1 order of magnitude separated the fastest and the slowest processes. The values of each time constant are listed in the legend of Figure 10.

If we look carefully at the impulse response function, we can observe however that it is not zero at time zero. This could be due to two reasons. The first one could be the presence of a weak residual emission of the donor at the observation wavelength. We have already ruled out this possibility since no significant residual fluorescent emission of the tryptophan residues is observed at the maximum emission wavelength of the acceptor, where the time-resolved experiments are performed (Figure 7A). The second reason, which is more likely, could be the existence of fast transfer kinetics, not resolvable by our instrumentation (<50 ps), which would account for a significant part of the transfer mechanism: 67%, 53%, and 30% of the peak intensity for the in vitro FpvA−PaA and FpvA−PaA−Ga^{3+} preparations and the in vivo FpvA−PaA preparation, respectively. This would mean that there are one or more donors so close to the acceptor, e.g., right in the binding site, that energy transfer is essentially instantaneous in the subnanosecond time scale.

This might explain the rather specific effect of PaA binding on the excited-state lifetime distribution, which concerned mainly the short excited-state lifetimes (Figure 8). These short excited-state lifetimes could therefore correspond to those Trp emitters mentioned above, close enough to PaA to be involved in an efficient FRET process. The disappearance of the ~100 ps excited-state lifetime could be explained by the competition with the short transfer time constants, either the measurable one of ~100 ps, identical to the short excited-state lifetime, or those shorter than the time resolution of the instrument. The value of this lifetime will be reduced by one-half since the lifetime of the donor in the presence of the acceptor is the harmonic sum of the lifetime in the absence of donor and of the energy transfer time constant. This gives a τ value of ~50 ps, which will be difficult to be confidently resolved. Since the excited-state lifetime τ_0 in the absence of donor displays a value similar to that of the measurable shortest transfer time constant (~100 ps), the interchromophore distance will be equal to R_0. This R_0 value corresponding to this short excited-state lifetime, computed from the value of the overlap integral J_λ and a donor quantum yield of 0.005 [calculated from the excited-state lifetime value of 110 ps in the absence of the acceptor and an intrinsic lifetime value of NATA of 21 ns (*31*)], will be ~13 Å. If faster transfer rates exist, as we assume, the effect on the lifetime values will be even stronger and shorter distances could be found.

The Size of the Detergent−FpvA Complexes. The long rotational correlation time measured by fluorescence anisotropy provided a mean value taken over all the complexes of 120 ± 23 ns (Table 3). This corresponds to a spherical rotating body with a hydrated volume (V_h) of 4.85 × 10^5 $Å^3$, which is much larger than the volume of the FpvA molecule (MW = 86 kDa, $V_{nonhydrated}$ = 1.04 × 10^5 $Å^3$, V_h = 1.47 × 10^5 $Å^3$ for a hydration ratio of 0.3 w/w). If we assume that the detergent/protein ratio is 1 w/w, as for FhuA (*32*), a Brownian rotational correlation time of 120 ns could be explained by a FpvA−detergent complex containing two FpvA and about 200 detergent molecules.

DISCUSSION

PaA, the major siderophore released by *P. aeruginosa* in iron limitation conditions, consists of a fluorescent chromophore (a derivative of 2,3-diamino-6,7-dihydroxyquinoline) linked to an 8 amino acid peptide (Figure 1). The changes in the fluorescence properties of PaA in solution with pH described are consistent with the well-characterized protonation states of PaA (*19*). In acidic conditions, a unique form of PaA, fully protonated, was observed. A single coordination state with the same lifetime as for the protonated form was observed for the metallic complexes (PaA−Ga^{3+} and PaA−Al^{3+}). As all pyoverdins secreted by fluorescent *Pseudomonads* share the same or very closely related highly fluorescent chromophore, the fluorescent properties described above for the PaA siderophore released by *P. aeruginosa* may be ascribed to all pyoverdins.

As documented previously (*13*), two procedures can be used to prepare the FpvA−PaA complex. Either the complex is preformed in vivo from a *P. aeruginosa* PaA- and FpvA-producing strain and subsequently purified, or it is prepared in vitro, starting with a purified empty receptor which is incubated with apo-PaA. For technical reasons, receptor−siderophore−metal complexes could only be prepared in vitro by incubating purified FpvA in the presence of PaA−metal. The dihydroquinoline moiety displayed almost the same excited-state lifetime in all the complexes studied. This value was slightly higher than for PaA itself in solution at pH 4 or when complexed with a metal (either at pH 7 or at pH 8.5). This is particularly informative, as it implies that, in the FpvA−PaA complexes, the bound iron-free PaA molecule is fully coordinated by charged groups in the protein binding site or is fully protonated. However, the local environment of the chromophore differs from one receptor−siderophore complex to the other. The most striking result is that the environment of PaA bound to FpvA differed, depending on how the complex was formed. The PaA in its binding site in the in vivo formed complex appeared to be in a less polar environment, to be less accessible to aqueous solutes, and to be more immobilized than in the in vitro formed FpvA−PaA complex. Although the metal complexes were also formed in vitro, the presence of the metal also decreased the accessibility of the chromophore to aqueous solute, the polarity of its environment, and its rotational mobility as compared to those of PaA in the in vitro formed FpvA−PaA complex, but to a lesser extent than for the in vivo preformed complex.

FRET measurements, using tryptophan and PaA as donor and acceptor, respectively, further confirmed these conformational differences. Three energy transfer time constants could be detected for the FRET occurring in the in vivo formed FpvA−PaA complex, compared to only two for the in vitro complexes (whether the metal is present or not). Moreover, faster transfer time constants (<50 ps) are probably present in each system where they can represent a substantial part of the total process. This heterogeneity of energy transfer kinetics can probably be ascribed to heterogeneity of the donors, as the FpvA protein contains 17 Trp residues. It is likely that several families of Trp−PaA couples are present with particular emission spectra, quantum yields, intrinsic lifetimes, and orientation−distance parameters. The existence of discrete FRET kinetic constants suggests a limited number of efficient donor−acceptor pairs (*33*). Although a lack of precise knowledge of the quantum yields and emission spectra of each Trp involved in the transfer process precludes a precise calculation of the PaA−Trp separations, the global fluorescence decay of FpvA, exhibiting four broad lifetime distributions, can be used, together with the FRET time constant values measured directly by monitoring the acceptor decay after indirect excitation, to restrict the range of critical distances within which the transfer will be the most efficient. The longest lifetimes, which we expected a priori to be the most efficient donors, since they display the highest quantum yields, are only marginally affected by the FRET. They are therefore likely associated with the most distant Trp residues. The shortest one (∼100 ps), on the contrary, disappears or is reduced in such a way that it is not measurable anymore in three out of four FpvA−PaA complexes. The R_0 value of ∼13 Å characterizes likely this (or these) short emitting Trp(s) exhibiting the strongest transfer efficiency and can be assumed as an upper limit since faster FRET are likely present.

Although FpvA displays only 22% homology with FhuA, the ferrichrome receptor, and although a full model of the structure of FpvA could not be determined from the X-ray structure of FhuA, some insight as to the location of the pyoverdin binding site can be obtained from sequence alignments and models. These methods enabled us to design a reasonable model of the FpvA cork structure and of the corresponding part of the β-barrel involved in FhuA in ferrichrome binding (data not shown). This indicates that the PaA binding site on FpvA is located in an equivalent position with respect to the barrel and the cork as compared to ferrichrome on FhuA. The estimated R_0 for the strongest transfer processes excluded 14 Trp residues, leaving only four putative candidates for the FRET with bound PaA. One of these Trp (Trp_{246} in FhuA corresponding to Trp_{321} in FpvA) is conserved in the two receptors and localized in the ferrichrome binding site. The nonconserved one, Trp_{391}, is also located within the binding site according to previously sequence alignments (*34*) and mutagenesis studies on FpvA (*35*). Two other tryptophans (Trp_{345} and Trp_{348}) could not be excluded on the basis of our distance criteria. All of these Trps are localized in flexible loops, and their conformation is probably modified in vivo.

The data presented here clearly show that the proteic environment of PaA in the FpvA−PaA−metal complexes is different from that in the FpvA−PaA complexes. This raises the question as to whether FpvA possesses either distinct binding sites or a single one which can adopt different conformations. Binding experiments in vitro on purified FpvA with PaA−$^{55}Fe^{3+}$ showed linear Scatchard representation with a stoichiometry of 0.83 (*13*), i.e., a single binding site for the PaA−Fe^{3+} complex, and a dissociation constant of 14 nM. Iron-free PaA displayed a similar K_d and can fully compete with PaA−Fe^{3+} in vitro (*13*) and in vivo (*15*). In the present paper, the determination of the inhibition constant of PaA−Al^{3+} and PaA−Ga^{3+} shows that these complexes compete as well with PaA−Fe^{3+} on FpvA. All of these binding and competition studies using [^{3}H]PaA or [^{3}H]PaA−Fe^{3+} did not reveal any ternary complex formation between two molecules of pyoverdin bound to one FpvA. Other data in the literature on different systems suggest that two binding

sites could be involved in transport. Mutagenesis studies on FepA suggested the existence of dual ligand binding sites for ferric−enterobactin, with the secondary site located deeper inside the protein (*36*). Consistent with these data, Payne and co-workers showed that the binding of ferric−enterobactin to its receptor occurs in at least two steps (*37*). Considering all of these data, if two different kinds of binding sites exist on FpvA, they should be mutually exclusive, binding to one site and completely abrogating binding to the other. Structural data support nevertheless the conformation change hypothesis. For instance, the FecA−ferric citrate X-ray structure shows large changes in the conformations of the extracellular loops of the β-barrel when ferric citrate binds to the receptor (*12*). Movements of the extracellular loops of FpvA could explain as well the difference in solvent accessibility and environmental polarity for the observed conformations of FpvA−PaA in the presence or absence of metal, and this condition is consistent with the existence of a single binding site able to take up different conformations.

The function of PaA in the FpvA−PaA complex is probably different from the one in the FpvA−PaA−metal complex. Indeed, the FpvA−PaA complex, in contrast to the FpvA−PaA−Fe^{3+} complex, is not competent for translocation through the outer membrane. Moreover, FpvA belongs to a subset of siderophore receptors (such as FecA in *E. coli* and PupB in *Pseudomonas putida*). The binding of the iron-free siderophore to these receptors induces the expression of the genes responsible for siderophore uptake (reviewed in ref *17*), a process that can be separated from the transport of the siderophore across the outer membrane. Therefore, these two separate activities might arise from two types of complexes, possessing either independent binding sites which are mutually exclusive as described above or one binding site exhibiting two different conformations.

The existence of the two different states of the FpvA−PaA complex described in this paper raises a question about which additional factor from the bacterium triggers a more buried location of PaA on its receptor in vivo. There is some evidence that this factor is TonB. We have shown previously that TonB regulates the kinetics of the formation of the FpvA−PaA−Fe^{3+} complex during iron uptake (*13*, *14*), although TonB does not affect the affinity of PaA or PaA−Fe^{3+} to FpvA (*14*). Moreover, in *E. coli*, alterations in the TonB boxes of ferric−siderophore receptors (*38*, *39*) and the absence of the TonB protein (*40*) affect the kinetics of ferric−siderophore binding and release as well as the displacement of the ferric−siderophore by phages. Considering these different effects of TonB, we suggest that the conformation observed for the in vivo formed FpvA−PaA complex is a TonB-induced conformation, where the PaA is located deeper inside the FpvA protein. To clarify the effect of TonB, the next step in this time-resolved fluorescence study will be to compare the fluorescent properties of FpvA−PaA complexes with those of the ternary TonB−FpvA−PaA complexes.

Taking together all of these data, it is clear that the FpvA receptor is able to interact in different ways with PaA, depending of the presence or not of metal or the way the complexes are prepared (in vivo or in vitro). All of the conformations described in this paper have certainly a biological function either in the PaA−Fe^{3+} uptake or in the regulation of the expression of genes involved in the iron uptake.

ACKNOWLEDGMENT

We are grateful to Professor J. R. Lakowicz for the kind gift of a sample of DCS. We thank the technical staff of LURE for running the synchrotron ring during the beam sessions. J.G. acknowledges A. Lukăs and Pr. B. Somogyi from the University of Pécs (Hungary) for helpful discussions and advice concerning the FRET with multiple donors.

REFERENCES

1. Poole, K., Neshat, K., and Heinrichs, D. E. (1993) *J. Bacteriol. 175*, 4597−4606.
2. Kadner, R. J. (1990) *Mol. Microbiol. 4*, 2027−2033.
3. Postle, K. (1993) *J. Bioenerg. Biomembr. 25*, 591−601.
4. Bradbeer, C. (1993) *J. Biol. Chem. 175*, 3146−3150.
5. Larsen, R. A., and Postle, K. (2001) *J. Biol. Chem. 276*, 8111−8117.
6. Larsen, R. A., Myers, P. S., Skare, J. T., Seachord, C. L., Darveau, R. P., and Postle, K. (1996) *J. Bacteriol. 178*, 1363−1373.
7. Coggshall, K. A., Cadieux, N., Piedmont, C., Kadner, R. J., and Cafiso, D. S. (2001) *Biochemistry 40*, 13964−13971.
8. Koster, W., and Bradbeer, C. (2001) *Res. Microbiol. 152*, 291−301.
9. Ferguson, A. D., Hofmann, E., Coulton, J. W., Diederichs, K., and Welte, W. (1998) *Science 282*, 2215−2220.
10. Locher, K. P., Rees, B., Koebnik, R., Mitschler, A., Moulinier, L., Rosenbusch, J. P., and Moras, D. (1998) *Cell 95*, 771−778.
11. Buchanan, S. K., Smith, B. S., Venkatramani, L., Xia, D., Esser, L., Palnitkar, M., Chakraborty, R., van der Helm, D., and Deisenhofer, J. (1999) *Nat. Struct. Biol. 6*, 56−63.
12. Ferguson, A. D., Chakraborty, R., Smith, B. S., Esser, L., van der Helm, D., and Deisenhofer, J. (2002) *Science 295*, 1715−1719.
13. Schalk, I. J., Kyslik, P., Prome, D., van Dorsselaer, A., Poole, K., Abdallah, M. A., and Pattus, F. (1999) *Biochemistry 38*, 9357−9365.
14. Schalk, I. J., Hennard, C., Dugave, C., Poole, K., Abdallah, M. A., and Pattus, F. (2001) *Mol. Microbiol. 39*, 351−361.
15. Schalk, I. J., Abdallah, M. A., and Pattus, F. (2002) *Biochemistry 41*, 1663−1671.
16. Gensberg, K., Hughes, K., and Smith, A. W. (1992) *J. Gen. Microbiol. 138*, 2381−2387.
17. Braun, V. (1997) *Arch. Microbiol. 167*, 325−331.
18. Demange, P., Bateman, A., Mertz, C., Dell, A., Piemont, Y., and Abdallah, M. A. (1990) *Biochemistry 29*, 11041−11051.
19. Albrecht-Garry, A. M., Blanc, S., Rochel, N., Ocacktan, A. Z., and Abdallah, M. A. (1994) *Inorg. Chem. 33*, 6391−6402.
20. Ankenbauer, R., Hanne, L. F., Cox, C. D., Hennard, C., Truong, Q. C., Desnottes, J. F., Paris, J. M., Moreau, N. J., and Abdallah, M. A. (1986) *J. Bacteriol. 167*, 7−11.
21. Livesey, A. K., and Brochon, J.-C. (1987) *Biophys. J. 52*, 693−706.
22. Vincent, M., and Gallay, J. (1991) *Eur. Biophys. J. 20*, 183−191.
23. Vincent, M., Gallay, J., and Demchenko, A. D. (1995) *J. Phys. Chem. 99*, 14931−14941.
24. Stryer, L. (1966) *J. Am. Chem. Soc. 88*, 5708−5712.
25. Viard, M., Gallay, J., Vincent, M., Meyer, O., Robert, B., and Paternostre, M. (1997) *Biophys. J. 73*, 2221−2234.
26. Macgregor, R. B., and Weber, G. (1986) *Nature 319*, 70−73.
27. Eftink, M. R. (1991) in *Topics in Fluorescence Spectroscopy* (Lakowicz, J. R., Ed.) pp 53−126, Plenum Press, New York and London.
28. Johnson, D. A., and Yguerabide, J. (1985) *Biophys. J. 48*, 949−955.
29. Stryer, L. (1978) *Annu. Rev. Biochem. 47*, 819−846.
30. Birks, J. B. (1970) *Photophysics of Aromatic Molecules*, Wiley-Interscience, John Wiley & Sons, Ltd., London, New York, Sydney, and Toronto.
31. Werner, T. C., and Forster, L. S. (1979) *Photochem. Photobiol. 29*, 905−914.
32. Boulanger, P., le Maire, M., Bonhivers, M., Dubois, S., Desmadril, M., and Letellier, L. (1996) *Biochemistry 35*, 14216−14224.

33. Somogyi, B., Lakos, Z., Szarka, A., and Nyitrai, M. (2000) *J. Photochem. Photobiol., B 59*, 26−32.
34. Folschweiller, N., Schalk, I. J., Celia, H., Kieffer, B., Abdallah, M. A., and Pattus, F. (2000) *Mol. Membr. Biol. 17*, 123−133.
35. Kilburn, L., Poole, K., Meyer, J. M., and Neshat, S. (1998) *J. Bacteriol. 180*, 6753−6756.
36. Cao, Z., Qi, Z., Sprencel, C., Newton, S. M., and Klebba, P. E. (2000) *Mol. Microbiol. 37*, 1306−1317.
37. Payne, M. A., Igo, J. D., Cao, Z., Foster, S. B., Newton, S. M., and Klebba, P. E. (1997) *J. Biol. Chem. 272*, 21950−21955.
38. Ferguson, A. D., Chakraborti, R., Smith, B. S., Esser, L., van der Helm, D., and Deisenhofer, J. (2002) *Science 295*, 1715−1719.
39. Reynolds, P. R., Mottur, G. P., Bradbeer, C., Scott, D. C., Cao, Z., Qi, Z., Bauler, M., Igo, J. D., Newton, S. M., and Klebba, P. E. (1980) *J. Biol. Chem. 255*, 4313−4319.
40. Gudmundsdottir, A., Bell, P. E., Lundrigan, M. D., Bradbeer, C., and Kadner, R. J. (1989) *J. Bacteriol. 171*, 6526−6533.
41. Frost, G. E., and Rosenberg, H. (1975) *J. Bacteriol. 124*, 704−712.
42. Kinosita, K. J., Kawato, S., and Ikegami, A. (1977) *Biophys. J. 20*, 289−305.
43. Berberan-Santos, M. N., and Valeur, B. (1991) *J. Chem. Phys. 95*, 8048−8055.

BI0259711